Exciton radiative properties in nonpolar homoepitaxial ZnO/(Zn,Mg)O quantum wells

L. Béaur,[1,2] T. Bretagnon,[1,2] B. Gil,[1,2,*] A. Kavokin,[1,2] T. Guillet,[1,2] C. Brimont,[1,2] D. Tainoff,[3] M. Teisseire,[3] and J.-M. Chauveau[3,4]

[1] *Université Montpellier 2, Laboratoire Charles Coulomb, UMR5221, F-34095 Montpellier, France*

[2] *CNRS, Laboratoire Charles Coulomb, UMR5221, F-34095 Montpellier, France*

[3] *CRHEA–CNRS, Rue Bernard Grégory, F-06560 Valbonne, France*

[4] *University of Nice Sophia Antipolis, Physics Dept., Parc Valrose, F-06102 Nice Cedex 2, France*

(Received 13 April 2011; revised manuscript received 24 June 2011; published 7 October 2011)

Photoluminescence spectra of nonpolar *M*-plane ZnO/$Zn_{0.8}Mg_{0.2}O$ quantum wells exhibit strong excitonic peaks from low (10 K) to high (325 K) temperatures. We find that the total integrated intensity remains quasiconstant and that the exciton lifetime increases linearly with the temperature from a value of 750 ps at 100 K until about 2.4 ns at 325 K. This behavior is well described by an original model accounting for the exciton phase space filling. This indicates that radiative recombination of free excitons is dominating the quantum well photoluminescence even at room temperature.

DOI: 10.1103/PhysRevB.84.165312 PACS number(s): 78.55.Et, 78.47.jd

I. INTRODUCTION

The quest for realizing compact solid state emitters in the UV-visible border has boosted the research on wurtzitic semiconductors during the last two decades. Group III nitrides and group II oxides are the two families of materials that are currently candidates to achieve this goal. Owing to the demonstrated *p*-type doping of nitrides, high-power blue light-emitting diodes and solid-state lasers based on nitrides are commercially available. The wurtzite structure of III nitrides and II oxides imposes significant constraints to their functionality. For instance, wurtzite semiconductors are subject to a spontaneous polarization in the [0001] direction,[1] in addition to their nonvanishing piezoelectric tensor. Thus, heterostructures based on such materials may display on-axis internal electric fields if assembled along the [0001] direction.[2–6] Under the influence of this electric field, electrons and holes in quantum wells experience a spatial separation. This results in more or less pronounced distortions of their envelope functions and a red shift of their recombination energy.[7] This phenomenon is known as a quantum confined Stark effect (QCSE). This electric-field-induced spatial separation of carriers having different charges induces a decrease of the overlap between the electron and hole ground-state wave functions, which may hinder obtaining an efficient light-matter interaction.[8] QCSE represents a very well-documented research area in group III nitride compounds, and it has only started being studied in group II oxide compounds.

In order to avoid the quantum confined Stark effect, the growth of heterostructures having wurtzite crystal symmetry on other than (0001) crystallographic planes has been proposed.[9] Among the most promising are the nonpolar planes,[10] such as the *M* plane (10-10) or *A* plane (11-20).[11] There is no component for the spontaneous polarization field in these orientations since the polar *c* axis lies in the growth plane. Nevertheless, in III nitrides, the performances of devices based on nonpolar materials are still limited due to various material problems, such as high densities of structural defects (e.g. stacking faults or dislocations).[11] Concerning the II-VI compounds, there are much fewer reports on the physics of nonpolar heterostructures[12–17] due to the lower maturity of research in this field.

In this paper, we analyze the optical properties of several homoepitaxial ZnO/$Zn_{0.8}Mg_{0.2}O$ single quantum wells (QWs) grown on an *M*-plane ZnO substrate. We examine the low-temperature (10 K) reflectance, and both continuous-wave photoluminescence (CW-PL) and time-resolved photoluminescence (TRPL) from 10 K up to 325 K. At low temperature, the reflectance and PL spectra exhibit strong in-plane polarization dependence.[17] The optical selection rules revealed experimentally are in agreement with the prediction of group theory. We report on the observation of the radiative recombination of free excitons (FEs) as well as the observation of radiative recombination of excitons localized on topological defects (LEs). The total PL intensity is kept almost constant until 325 K, which indicates the absence of nonradiative recombination channels in the samples. To show quantitative and experimental evidence of this remarkable property of such quantum wells, the lifetimes of free and localized excitons are accurately measured by TRPL. They are found to increase linearly from ∼750 ps to ∼2.4 ns when the temperature varies in the range from 100 to 325 K. Both decay times show an identical behavior with temperature, which is fully compatible with the thermal populations of the two PL bands. The radiative decay time of the free exciton tends toward the theoretically expected value of several picoseconds at 0 K, which is evidence of a high in-plane mobility of the excitons in our samples. Experiments discussed in detail here are performed on a 1.7-nm-wide quantum well. The measured linear temperature increase of the radiative decay time of free excitons is about 7 ± 1 ps/K. The evolution of the radiative decay time with temperature is computed in the context of a modified version of the model developed for GaAs/(Al,Ga)As square quantum wells.[18–22] This model has been previously used to successfully interpret the temperature dependence of radiative decay times of high-quality GaN/(Al,Ga)N quantum wells.[18] Here, in addition, we extend this model to the case of quantum wells for which the energy dispersion relations display in-plane anisotropy. We show that the material parameters allow us to use approximate analytical expressions with good accuracy.

The agreement we find between experiment and theory is excellent.

II. SAMPLES

Homoepitaxial QW samples were grown in a Riber Epineat MBE system equipped with effusion cells for Zn and Mg elements. Atomic oxygen was supplied via an Addon radio-frequency (rf) plasma cell using an rf power of 320 W with an O flux of 1.0 sscm. The nonpolar heterostructures were grown on 10 × 20 mm^2 *M*-plane ZnO substrates. Before the growth of the active layer, the substrate was annealed inside the growth chamber at ∼800 °C for 1 h under O plasma. A 2-nm ZnO buffer layer was grown at 400 °C and annealed for 30 min at 800 °C under O flux. After this annealing step, a streaky pattern was observed by reflection high-energy electron diffraction (RHEED) along the two orthogonal in-plane directions (parallel and perpendicular to the *c* axis). The growth of the ZnO/(Zn,Mg)O QW heterostructure was then performed under slightly rich metal conditions with a growth rate of ∼0.2 μm/h. Before growing the active layers, a 150-nm (Zn,Mg)O buffer layer was deposited. The QWs had thicknesses ranging between 1.7 and 3.5 nm.[17] A 50-nm (Zn,Mg)O cap layer was finally grown on top of the structure. The Mg concentration was measured to be ∼20% for all samples. The optical properties of these quantum wells were rather similar, and we will restrict this paper to investigation carried out on the 1.7-nm thin quantum well.

III. OPTICAL SPECTROSCOPY

The samples were studied by means of reflectivity, continuous-wave photoluminescence (CW-PL), integrated time resolved photoluminescence (ITRPL), and time-resolved photoluminescence (TRPL) techniques. The samples were mounted in a helium flow cryostat for all of these measurements. The temperature varied from 10 to 325 K. For reflectivity and CW-PL, the light sources were a Xenon lamp and a helium-cadmium laser at 325 nm, respectively. The laser beam was focused onto the samples to a 100-μm-diameter spot with an average power of 5 mW. The quantum well luminescence and reflectivity were analyzed using a 550-mm monochromator and a CCD-camera. For TRPL experiments, the excitation source was provided by a mode-locked frequency tripled titanium-sapphire laser, with a 2-ps pulse width and a wavelength of 260 nm. The focused laser spot diameter was also 100 μm. In addition, due to the slowness of the observed decays, we have adapted the laser repetition rate between 82 MHz and 800 Hz by using an acousto-optic modulator. The PL signal was dispersed by an imaging spectrometer and then temporally resolved by a streak camera with an overall time resolution of 8 ps.

A. Optical spectroscopy results

Figure 1 shows CW-PL and normal incidence reflectivity spectra of a 1.7-nm-thick quantum well taken at 10 K for two polarizations (*E*//*c* axis and *E*⊥*c* axis). As expected from the growth plane symmetry, strong in-plane optical anisotropies are revealed. Indeed, excitons having the Γ_5 symmetry couple with an electromagnetic field perpendicular to the *c* axis,

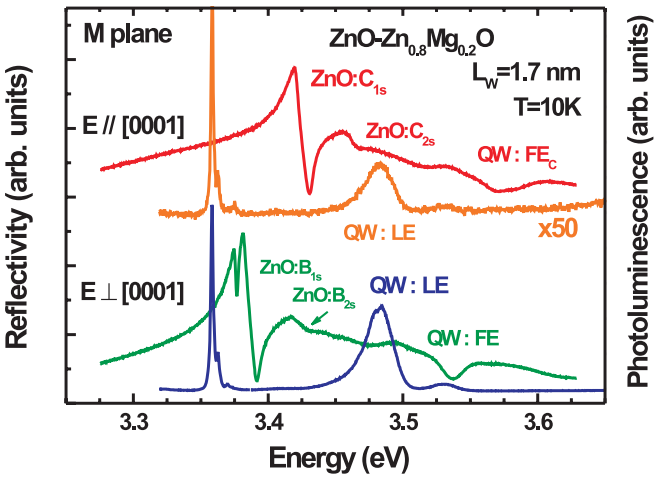

FIG. 1. (Color online) Low temperature polarized (red and green plots) reflectance spectra of a 1.7-nm thin ZnO/$Zn_{0.8}Mg_{0.2}O$ single quantum well grown on an *M*-plane-oriented ZnO substrate showing the excitonic selection rules. Low-temperature PL spectra (blue and orange plots) showing both FE and LE. Note the efficient thermalization of the carriers into the low-energy states in all PL spectra.

whereas only excitons having the Γ_1 symmetry couple with an electromagnetic field parallel to the *c* axis.[23]

Both 1*s* and 2*s* states of C excitons from the bulk ZnO substrate are observed in the reflectivity spectrum where light is polarized in [0001] direction (red line plot). The high-energy structure located at 3.57 eV is attributed to the confined state analogous to a C exciton in bulk ZnO. The spectrum collected in the orthogonal polarization is also plotted in the Figure (green). In that case, 1*s* A and B excitons as well as their 2*s* states are observed, together with a merged reflectivity resonance at 3.537 eV. This doublet structure is due to confined A and B excitons. The PL spectrum, plotted in blue, indicates a weak Stokes shift between PL (3.532 eV) and reflectivity (3.537 eV) as a probe of reasonable heterointerface smoothness with terraces of the size of the exciton Bohr radius.[24] The Stokes shift in QWs is expected to be due to the QW width fluctuations and possibly due to local built-in piezoelectric fields. A stronger lower-energy (3.483 eV) PL band that slightly reabsorbs light and thus gives a reflectance feature at 3.497 eV is also observed. The ∼50-meV splitting between these two structures is too large to be explained by one-monolayer QW width fluctuations as our envelope function calculation shows. From the complementary temperature-dependent photoluminescence intensity measurements and time-resolved spectroscopy data (detailed further in this paper), we attribute this line to topological defects. For the sake of completeness, we have also reported the photoluminescence spectrum detected in polarization perpendicular to the [0001] direction. In Fig. 1, the corresponding spectrum is magnified by a factor of 50. At 10 K, the C confined exciton is fully thermalized, and we only report weak photoluminescence signal at the band gap of ZnO. These efficient thermalization effects lead to low intensity of the quantum-well-related photoluminescence features, and prevent us from measuring decay times in this polarization. The PL intensity ratio between

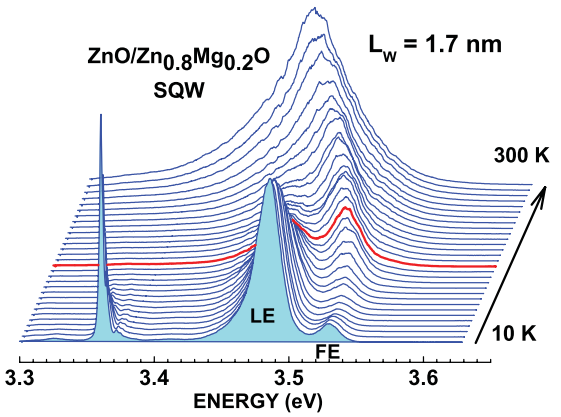

FIG. 2. (Color online) Evolution of the PL lines corresponding to confined free excitons and localized excitons in the case of a 1.7-nm thin $ZnO/Zn_{0.8}Mg_{0.2}O$ single quantum well grown on an *M*-plane-oriented ZnO substrate. Note the population exchange at ∼150 K (red).

the spectra taken in parallel and perpendicular polarizations is about 98%.

Figure 2 shows a series of CW-PL spectra measured at different temperatures changing in the range from 10 to 300 K. It is interesting to notice the inversion of the intensity ratio between the peaks associated to free and localized excitons at about 150 K, which indicates an efficient detrapping of the localized excitons. A clear splitting is observed up to 250 K. Then the two lines merge to form a broad luminescence band.

A deconvolution procedure of the photoluminescence band was performed in order to extract the energies of the two levels. Figure 3(a) shows the evolution of the photoluminescence energies with temperature. The energies of both free exciton transition and localized exciton one are described by a similar Varshni's law (dashed lines).[25] From these results, we can

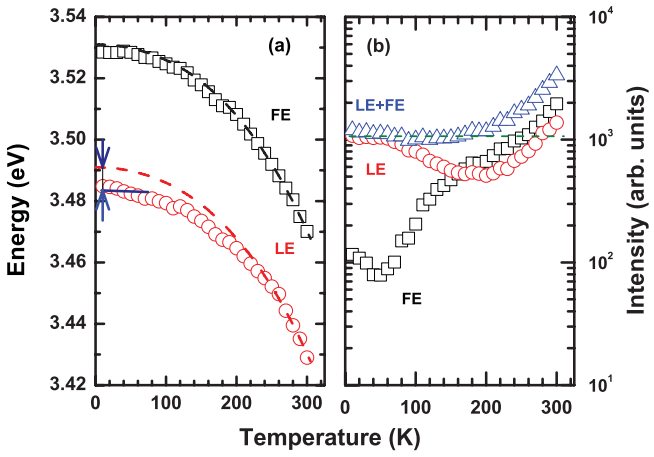

FIG. 3. (Color online) (a) Evolution of the energies in CW-PL measurement of free (open square) and localized (open circle) exciton bands with increasing temperature. The dashed lines are Varshni's law. (b) Evolution of the intensities in CW-PL measurement of free (open square) and localized (open circle) exciton bands together with the total photoluminescence intensity (open triangle) with increasing temperature.

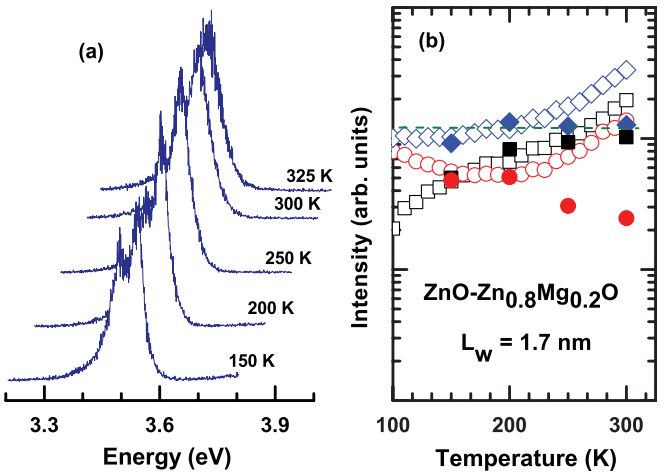

FIG. 4. (Color online) (a) Evolution of the ITRPL spectra for different temperatures ranging from 150 to 325 K. Note that the intensity does not change when temperature increases. (b) Same figure as Fig. 3(b), but we add the evolution of the intensities in ITRPL measurement of free (full square) and localized (full circle) exciton bands together with the total photoluminescence intensity (full triangle) with temperature.

deduce the localization energy of the exciton in the 10 meV range. In Fig. 3(b), the intensities of these two peaks as well as the total PL intensity are plotted. At low temperature, the intensity of the localized exciton line remains nearly constant, while the intensity of the free exciton line slightly decreases. At 60 K, the intensity of the FE line starts to increase, and the intensity of the LE line begins to decrease. At 150 K, both lines have the same intensity. This is a clear indication of the thermal detrapping of the localized exciton state and population of the free exciton state induced by the temperature increase. For the temperatures above 220 K, an increase of the sum of two peak intensities is observed. This is an experimental artifact. It is due to the difference between the energy of the excitation (3.8 eV in CW-PL) and the band gap of the barrier, which decreases from 3.85 eV at low temperature to 3.77 eV at room temperature. It is thus correlated to the experimental excitation conditions, which makes the band gap of (Zn,Mg)O pass through the value of the laser energy when red shifting with temperature. This results in the modified absorption and varying densities of photo-generated carriers. If using a higher photon energy $E_{laser} > E_{barrier}$, as in the TRPL experiment (excitation energy now sitting at 4.71 eV), there is no longer any significant changes in (Zn,Mg)O absorption between low and room temperature, and this behavior is not observed. This is demonstrated in Fig. 4(a), where the constant intensity of the PL obtained after integration of the PL spectra taken at different times is shown for temperatures ranging up to 325 K. For the sake of demonstration, we plot in Fig. 4(b) the intensities of both lines and their sum (full symbols) in comparison with the CW-PL results. It is worthwhile noticing that the total photoluminescence intensity does not collapse at high temperatures, as shown in Fig. 4(b). This is a clear indication that nonradiative processes are not efficient, even beyond the room temperature conditions, which is extremely promising for optoelectronic devices.

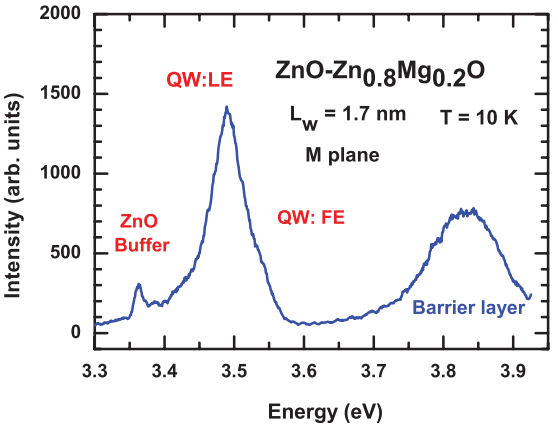

FIG. 5. (Color online) Low-temperature unpolarized PL spectrum of a 1.7-nm thin $ZnO/Zn_{0.8}Mg_{0.2}O$ single quantum well grown on an *M*-plane ZnO substrate. The PL of the barrier layers exhibits a low-energy wing that extends more or less down to the quantum well PL energy. The quantum-well-related PL is composite with an FE contribution at high energy and the signature of an LE at lower energy.

Figure 5 illustrates the crystalline quality of the $Zn_{0.8}Mg_{0.2}O$ barrier layer that is revealed via the line shape of its 10-K photoluminescence. A very low line broadening indicates that the barrier layer is quite homogeneous in the studied sample. The photoluminescence tail extends towards the low energy side down to the quantum-well-related photoluminescence line. This indicates that leakages of excitons and photo-created carriers may impact on the evolution of PL spectra as a function of temperature or time. Special care needs to be taken about this. The exciton leakage prevents us from deducing accurately the exciton radiative decay times at low temperatures, where the characteristic recombination times are very short.

B. Photoluminescence decay times

Figure 6 shows some typical PL decays in the barrier and in the quantum well measured at 10 K in the two different time scales: (a) 1 μs and (b) 5 ns. These spectra correspond to different experiments. At this temperature, the exciton contribution to the PL spectra of the QWs is not easy to extract. A very long PL transient is characteristic of these PL spectra. The observed decay is similar to the decay of photoluminescence in the barrier spectral region. At low temperature, the QW PL decay is dependent on several factors, and its detailed analysis is beyond the scope of this paper. At temperatures above 100 K, the barrier-related PL line collapses due to the nonradiative processes in the barrier layer. We therefore restrict ourselves in this paper to the study of decay times measured at higher temperature.

Figure 7 displays the normalized PL decays of the free and localized exciton-related PL bands at several temperatures ranging from 150 to 325 K. At these temperatures, the intensity of PL decreases monoexponentially with time. The decay times of free and localized excitons monotonically increase with temperature.

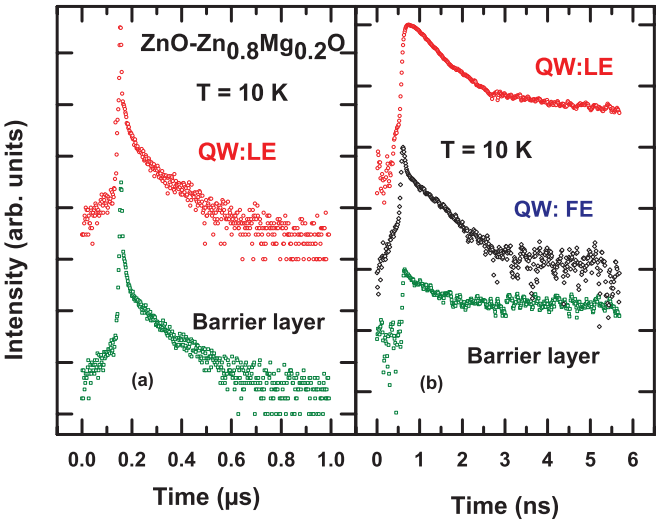

FIG. 6. (Color online) (a) PL normalized decay of the(Zn, Mg)O barrier and LE in the case of a 1.7-nm thin $ZnO/Zn_{0.8}Mg_{0.2}O$ single quantum well recorded on a 1-μs time scale. The scale on the vertical axis is logarithmic. (b) Similar results recorded on a 5-ns time scale. The PL decay of the FE is shown in this figure. The scale on the vertical axis is logarithmic.

In Fig. 8, the evolution of the radiative decay times for both free and localized excitons is shown. The data shift linearly with temperature within the limits of experimental accuracy and tend toward zero at 0 K. This linear increase of the decay time is typical of free excitons in QWs. The slope of about 7 ± 1 ps/K will be interpreted in the next section in the context of an original model accounting the in-plane anisotropy of the band structure. Note that a similar slope has been observed in GaN/(Al, Ga)N quantum wells[18] (11 ps/K).

IV. COMPARISON WITH A THEORETICAL MODEL

A theoretical model allowing calculation of free exciton radiative lifetimes as function of temperature and polarization

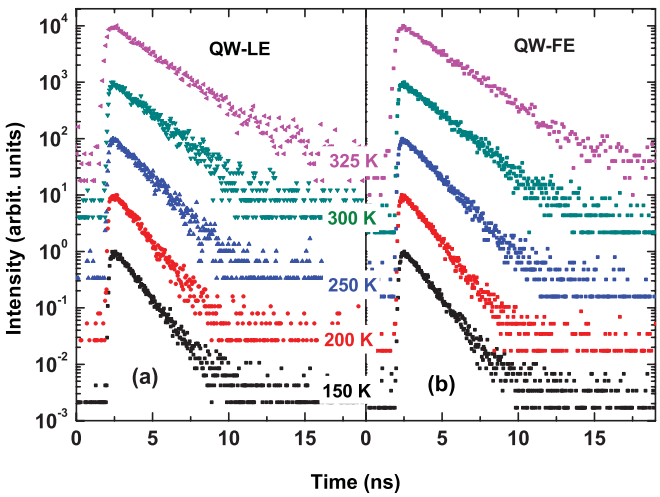

FIG. 7. (Color online) PL decay of (a) localized and (b) free excitons for a 1.7-nm thin $ZnO/Zn_{0.8}Mg_{0.2}O$ single quantum recorded at different temperatures ranging from 150 to 325 K.

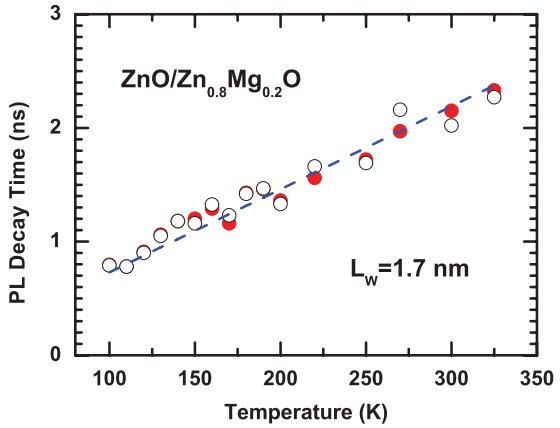

FIG. 8. (Color online) Evolution of the PL decay times of the localized (full symbol) and free excitons (open symbol) versus temperature.

is described in detail in the Appendix section of this paper. It is based on the assumption that only light emitted by excitons situated inside the light cone defined by the wave vector of light in vacuum is able to leave the structure through its surfaces.[26] The excitons having larger wave vectors either recombine nonradiatively or emit photons which remain in the structure and are eventually reabsorbed. In this section, we grossly evaluate quantities a and b in Eq. (A15) in order to obtain a simple analytical result for the slope of temperature dependence of the radiative lifetime.

The emission energy typical of ZnO/(Zn, Mg)O or GaN/(Ga, Al)N quantum wells sits near 3.6 eV, which corresponds to $\frac{\omega}{c} = k_0 \approx 2 \times 10^7 \mathrm{m}^{-1}$.

For the effective masses, we refer to the recent theoretical calculation of Yan *et al.*[27] In the context of this calculation, which neglects spin-orbit interaction (including it would not significantly impact the evaluations below but would prevent us from obtaining analytical expressions for the hole masses), the Γ_9 hole mass expressed in free electron masses are:

$$m_{\Gamma_{9z}} = \left| \frac{1}{A_1 + A_3} \right| = 2.73 \quad \text{and} \tag{1}$$

$$m_{\Gamma_{9y}} = \left| \frac{1}{A_2 + A_4 + A_5} \right| = 2.66. \tag{2}$$

The ZnO related values of the electron masses expressed in free electron mass are:[27] $m_e z = 0.246$ and $m_e y = 0.329$.

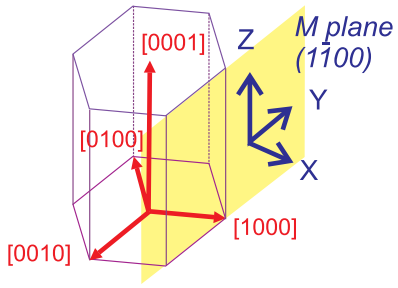

FIG. 9. (Color online) Schematic view of nonpolar M plane, direction x, y, and z corresponding the notation used in calculation. Note that the z direction corresponds to the crystal axis c.

Finally, we obtain $a \approx 1.4 \times 10^{-4}$ at 300 K. Concerning b, similar calculation leads us to $b \approx 3 \times 10^{-6}$ at 300 K.

Now we can rewrite equation (A18) as:

$$\Gamma(T) \approx \frac{k\omega_{\mathrm{LT}} a_B^3 I_{\mathrm{eh}}^2}{\lambda^2} \frac{\hbar^2\omega^2}{4c^2 k_B T} \left(\frac{1}{m_{ey} + m_{hy}} + \frac{1}{m_{ez} + m_{hz}} \right). \tag{3}$$

The temperature dependence of the radiative decays times finally expresses as:

$$\tau_{\mathrm{rad}}(T) \approx \frac{2c^2 k_B}{\hbar^2 k \omega_{\mathrm{LT}} a_B^3} \left(\frac{1}{m_{ey}+m_{hy}} + \frac{1}{m_{ez} + m_{hz}} \right)^{-1} \frac{\lambda^2}{\omega^2 I_{\mathrm{eh}}^2} T. \tag{4}$$

Using $n = 2.56$[28] and $\hbar\omega_{\mathrm{LT}} = 5$ meV,[29–32] we obtain a slope 10 psK^{-1}, which nicely matches with the experimental value.

It is important to account for the optical selection rules for excitons in bulk wurtzite crystals, which affect the values of the oscillator strengths, which are hidden in Eqs. (3) and (4) in the longitudinal-transverse splitting ω_{LT}. Let us, for instance, consider the A exciton. This exciton is forbidden in the polarization parallel to [0001] direction in bulk unstrained ZnO (or any other wurtzitic semiconductor), while it is a dipole allowed recombination (creation) process in other polarizations. Thus the value of ω_{LT}, which one needs to use in the expression for the decay time, depends on the configuration of the experiment. We should take $\omega_{\mathrm{LT}} \approx 0$ if measuring the photoluminescence decay times of free excitons in the polarization parallel to [0001] direction, whilst ω_{LT} should be given its experimental value in the case of an experiment performed in crossed-polarization conditions. Equations (A10) and (A11) indicate that the oscillator strengths of B and C excitons never vanish when φ changes. We emphasize that, for a detailed comparison of the experiment and theory, care has to be taken of the definition of ω_{LT} for Γ_5 excitons.[29–31]

V. CONCLUSIONS

The CW reflectance, CW photoluminescence, and time-resolved photoluminescence properties of ZnO-$Zn_{0.8}Mg_{0.2}O$ single quantum wells grown on M-plane-oriented ZnO substrates have revealed both free excitons (with a weak Stokes shift between reflectance and photoluminescence spectra) and localized excitons. These excitons are most probably trapped to topological defects. Complementary experiments, such as cathodoluminescence investigations, are needed to clearly identify their origin. Changing the lattice temperature, we find that a thermal equilibrium distribution governs the populations of both free excitons and localized excitons with a globally constant total intensity from 10 K up to 325 K. The constant intensity of the photoluminescence, whatever the temperature is, indicates the very moderate contributions of nonradiative recombination channels in these samples. The lifetimes of free excitons are very short and extremely difficult to measure at low temperature using our setup and due to the existence of low residual photoluminescence tail from the barrier layer and to complementary feeding of the quantum wells with carriers that escape from the barrier layer. We could not measure time-resolved photoluminescence by using an optical pump at the energies intermediate between the quantum well exciton

energy and the $Zn_{0.8}Mg_{0.2}O$ barrier exciton energy to get rid of these deleterious phenomena. The radiative decay times of the free excitons and of the localized excitons have been plotted as a function of the temperature. The radiative decay times of the free exciton asymptotically tend to the theoretical limit for an ideal free 2D exciton at 0 K, which is an indication of the high mobility of excitons in such samples. Above 100 K, the decay times of both free and localized excitons have identical values and similar slope with T. These behaviors are fully compatible with the thermal population of the two photoluminescence bands. Experiments carried on a series of quantum wells with well widths ranging from 3.5 nm down to 1.7 nm lead to the slope of temperature dependence of the radiative decay times of free excitons of typically 7 ± 1 psK^{-1}.

To interpret the evolution of the radiative decay time with temperature, we have successfully extended the model developed for GaAs/(Ga, Al)As quantum wells to the case of quantum wells having in-plane anisotropy of the energy dispersion relation. This model was previously used with success to interpret the temperature dependence of radiative decay times of the photoluminescence in many high-quality quantum well systems including GaN/(Ga, Al)N wells grown along the [0001] direction. The agreement between theory and experiment is excellent, which is an indication of the maturity of the homoepitaxial growth of ZnO/(Zn, Mg)O quantum well along nonpolar directions.

ACKNOWLEDGMENTS

The authors acknowledge financial support of ANR under the ZOOM project (Grant No. ANR-06-BLAN-0135), DefiZnO project (ANR-09-MAPR-009), and the collaboration project CEA/CNRS number C12899/047588.

APPENDIX: THEORETICAL MODEL FOR CALCULATION OF THE EXCITON RADIATIVE LIFETIME

The radiative recombination rate is calculated for all exciton states as a function of their polarization and wave vector. The average radiative lifetime is then calculated for a thermal population of excitons. We consider the excitons which can freely propagate in the quantum well plane (y, z). The exciton kinetic energy for the motion in y and z directions (see Fig. 9) is:

$$E_y(k_y) = \left(\frac{\hbar^2}{2(m_{ey} + m_{hy})}\right) k_y^2$$

and

$$E_z(k_z) = \left(\frac{\hbar^2}{2(m_{ez} + m_{hz})}\right) k_z^2. \tag{A1}$$

In Eq. (1), $m_e y$, m_{ez}, m_{hy}, and m_{hz} represent the masses of electron hole in the y and z directions, respectively.

Now we can write the kinetic energy of an exciton having an arbitrary oriented wave vector $\mathbf{k}$ in the plane (y, z) in terms of an angle φ:

$$k_y = k\cos\varphi, \qquad k_z = k\sin\varphi. \tag{A2}$$

The energy of the excitons at the border of the light cone is defined as:

$$E_c(\varphi) = E_y\left(\frac{\omega}{c}\cos\varphi\right) + E_z\left(\frac{\omega}{c}\sin\varphi\right) = \frac{\hbar^2 k^2}{2M(\varphi)}, \tag{A3}$$

where $\frac{\omega}{c} = k_0$ is the wave vector of light in vacuum at the exciton resonance pulsation ω, and $M(\varphi)$ is the φ-dependent exciton in-plane translation mass.

Now we account for the fact that only the excitons having their wave vectors inside the light cone may emit light. Their radiative decay rate is dependent on the polarization of emitted light, as it has been shown by several authors in the 1990s[18–22]. For the excitons polarized in the direction perpendicular to the wave vector (T polarization), the radiative decay rate increases with k as:[20,21]

$$\Gamma_0^T(k) = \frac{\Gamma_0(0)}{\sqrt{1 - \left(\frac{kc}{\omega n}\right)^2}}, \tag{A4}$$

where n is the background refractive index and where the recombination rate at $k = 0$, $\Gamma_0(0)$ expresses as a function of: a_B the Bohr radius in the bulk, ω_{LT} the excitonic longitudinal transverse splitting pulsation, λ a variational parameter corresponding to the two-dimensional confined Bohr radius, and I_{eh} the electron-hole envelope function integral:[22]

$$\Gamma_0(0) = \frac{k\omega_{LT} a_B^3 I_{eh}^2}{\lambda^2}. \tag{A5}$$

For the excitons polarized along the wave vector (L polarization), the radiative decay rate is:[20,21]

$$\Gamma_0^L(k) = \sqrt{1 - \left(\frac{kc}{\omega n}\right)^2}\,\Gamma_0(0). \tag{A6}$$

Finally, for the excitons polarized normal to the QW plane direction, the radiative decay rate is:[20,21]

$$\Gamma_0^\perp(k) = \frac{\left(\frac{kc}{\omega n}\right)^2 \Gamma_0(0)}{\sqrt{1 - \left(\frac{kc}{\omega n}\right)^2}}. \tag{A7}$$

Note that for these types of excitons, light can only be emitted at oblique angles, as there is no longitudinal light mode in vacuum. Having in mind that high oblique angles are inaccessible in planar semiconductor structures due the total internal reflection of light, emission of excitons polarized normal to QW plane direction is virtually zero. The integrated

decay rate of the thermal population of excitons in a quantum well is given by:

$$\Gamma(T) = \frac{\hbar^2}{k_B T}\frac{c^2}{\pi\omega^2}\sum_{i=T,L,\perp}\int_0^{\omega/c} kdk\int_0^{2\pi} d\phi \times \exp\left[-\frac{E_y(k\cos\phi)+E_z(k\sin\phi)}{k_B T}\right]\Gamma_0^i(k)\frac{g(i,\phi)}{M(\varphi)}, \tag{A8}$$

where k_B is the Boltzmann constant, M is the exciton effective mass, and the factor $g(I, \varphi)$ accounts for the polarization selection rules for a given exciton resonance.

In particular, for the exciton A:

$$g(T,\varphi) = \cos^2\varphi, \quad g(L,\varphi) = \sin^2\varphi, \quad g(\perp,\varphi) = 0. \tag{A9}$$

For the excitons B and C:

$$g_B(T,\varphi) = \xi^2\cos^2\varphi + \frac{1-\xi^2}{2}\sin^2\varphi,$$
$$g_B(L,\varphi) = \xi^2\sin^2\varphi + \frac{1-\xi^2}{2}\cos^2\varphi, \quad g_B(\perp,\varphi) = 0 \tag{A10}$$

and

$$g_C(T,\varphi) = \frac{1-\xi^2}{2}\cos^2\varphi + \xi^2\sin^2\varphi,$$
$$g_C(L,\varphi) = \frac{1-\xi^2}{2}\sin^2\varphi + \xi^2\cos^2\varphi, \quad g_C(\perp,\varphi) = 0 \tag{A11}$$

with

$$\xi = \frac{\sqrt{2}\Delta_3}{\sqrt{\left(\frac{\Delta_1-\Delta_2}{2} - \sqrt{\left(\frac{\Delta_1-\Delta_2}{2}\right)^2 + 2\Delta_3^2}\right)^2 + 2\Delta_3^2}}, \tag{A12}$$

where the Δ_i are, respectively, the valence band crystal field splitting ($i = 1$) and the two component spin-orbit interaction parameter ($i = 2, 3$).[25] In Eq. (A8), the integration is done within the light cone where excitons can directly emit light outside the structure through its surfaces. It is not that excitons having wave vectors $\omega/c < k < n\omega/c$ can still emit light through the sides of the sample. The radiative decay time for these excitons is much longer than of those having $k < \omega/c$, and it is strongly dependent on the sample geometry. In the present model, we assume it to be infinite.

We note that the wave vector dependence of the radiative decay rates given by Eqs. (A4) to (A7) is relatively weak inside the light cone ($0 < k < \frac{\omega}{c}$). If the exciton radiative decay rate Γ_0 is assumed to be independent on the in-plane wave vector, a quasianalytical expression can be obtained following Andreani *et al.*[20,26]

In order to quantify the impact of the φ-dependent exciton center-of-mass motion in the quantum well plane, let us assume Γ_0 to be k independent [$\Gamma_0^i(k) = \Gamma_0(0)\forall i$], so that we can get analytical expressions for the integral in Eq. (A8). Let us specifically consider the type A excitons for which the i summation over the $g(i, \varphi)$ given by Eq. (A9) gives its maximum value: 1.

Replacing in Eq. (A8) the integration over k by an integration over the energy leads to a vanishing of $(\frac{c}{\omega})^2$ and makes to appear $\frac{1}{2k_B T}$.

The fraction of excitons which may decay radiatively at temperature T is given by:

$$N(T) = \frac{1}{2\pi k_B T}\int_0^{2\pi} d\varphi\int_0^{E_c(\varphi)} dE\exp\left(-\frac{E}{k_B T}\right) = 1 - \frac{1}{2\pi}\int_0^{2\pi} d\varphi\exp\left(-\frac{E_c(\varphi)}{k_B T}\right), \tag{A13}$$

$$N(T) = 1 - \frac{1}{2\pi}\exp\left[-\frac{\hbar^2\omega^2}{4c^2 k_B T}\left(\frac{1}{m_{ey}+m_{hy}} + \frac{1}{m_{ez}+m_{hz}}\right)\right] \times \int_0^{2\pi}\exp\left[\frac{\hbar^2\omega^2}{4c^2 k_B T}\left(\frac{1}{m_{ey}+m_{hy}} - \frac{1}{m_{ez}+m_{hz}}\right)\times\cos 2\phi\right]d\phi, \tag{A14}$$

and

$$N(T) = 1 - \frac{1}{2\pi}e^{-a}\int_0^{2\pi} e^{b\cos 2\varphi}d\varphi. \tag{A15}$$

The integral $\int_0^{2\pi} e^{b\cos 2\varphi}d\varphi$ has to be computed numerically. We wish to point out here that, in Eq. (A15),

$$a = -\frac{\hbar^2\omega^2}{4c^2 k_B T}\left(\frac{1}{m_{ey}+m_{hy}} + \frac{1}{m_{ez}+m_{hz}}\right) \tag{A16}$$

represents the in-plane average of the excitonic translation mass, whilst

$$b = \frac{\hbar^2\omega^2}{4c^2 k_B T}\left(\frac{1}{m_{ey}+m_{hy}} - \frac{1}{m_{ez}+m_{hz}}\right) \tag{A17}$$

represents the anisotropy of this quantity.

The radiative decay rate is given by Eq. (A8), which reads now:

$$\Gamma(T) = \Gamma_0 N(T) \tag{A18}$$

and

$$\tau(T) = \frac{1}{2\Gamma_0 N(T)}. \tag{A19}$$

*Corresponding author: bernard.gil@univ-montp2.fr

[1] J. F. Nye, *Physical Properties of Crystals* (Oxford Science Publications, Oxford, 1957), p. 79.

[2] T. Takeuchi, S. Sota, M. Katsuragawa, M. Mori, H. Takeuchi, H. Amano, and I. Akasaki, Jpn. J. Appl. Phys. part 2 N°4A, **36**, L382 (1997).

[3] J. Seo Im, H. Kollmer, J. Off, A. Sohmer, F. Scholz, and A. Hangleiter, Phys. Rev. B **57**, R9435 (1998).

[4] M. Leroux, N. Grandjean, M. Laügt, J. Massies, B. Gil, P. Lefebvre, and P. Bigenwald, Phys. Rev. B **58**, R13371 (1999).

[5]C. Morhain, T. Bretagnon, P. Lefebvre, X. Tang, P. Valvin, T. Guillet, B. Gil, T. Taliercio, M. Teisseire-Doninelli, B. Vinter, and C. Deparis, Phys. Rev. B **72**, R241305 (2005).
[6]T. Bretagnon, P. Lefebvre, T. Guillet, T. Taliercio, B. Gil, and C. Morhain, Appl. Phys. Lett. **90**, 201912 (2007).
[7]G. Bastard, in *Wave mechanics applied to semiconductor heterostructures* (Les Editions de Physique, Paris, 1987), p. 303.
[8]P. Bigenwald, P. Lefebvre, T. Bretagnon, and B. Gil, Phys. Stat. Solidi (b) **216**, 371 (1999).
[9]T. Takeuchi, H. Amano, and I. Akasaki, Japan. J. Appl. Phys. Part 1 **39**, 413 (2000).
[10]P. Walterelt, O. Brandt, A. Trampert, H. T. Grahn, J. Mennlger, M. Ramstelner, M. Relche, and K. H. Ploog, Nature (London) **406**, 865 (2000).
[11]For a review, see *Nitrides with Non Polar Surfaces*, edited by Tanya Paskova (Wiley VCH, Weinheim, 2008), pp. 3–411.
[12]T. Moriyama and S. Fujita, Jap. J. Appl. Phys. **44**, 7919 (2005).
[13]J. M. Chauveau, D. A. Buell, M. Laugt, P. Vennegues, M. Teisseire-Doninelli, S. Berard-Bergery, C. Deparis, B. Lo, B. Vinter, and C. Morhain, J. Cryst. Growth **301**, 366 (2007).
[14]H. Matsui, N. Hasuike, H. Harima, and H. Tabata, J. Appl. Phys. **104**, 094309 (2008).
[15]T. S. Ko, T. C. Lu, L. F. Zhuo, W. L. Wang, M. H. Liang, H. C. Kuo, S. C. Wang, Li Chang, and D. Y. Lin, J. Appl. Phys. **108**, 073504 (2010).
[16]J.-M. Chauveau, M. Teisseire, H. Kim-Chauveau, C. Deparis, C. Morhain, and B. Vinter, Appl. Phys. Lett. **97**, 081903 (2010).
[17]L. Béaur, T. Bretagnon, C. Brimont, T. Guillet, B. Gil, D. Tainoff, M. Teisseire, and J. M. Chauveau, Appl. Phys. Lett. **98**, 101913 (2011).
[18]P. Lefebvre, J. Allegre, B. Gil, A. Kavokine, H. Mathieu, H. Morkoc, W. Kim, A. Salvador, and A. Botchkarev, Phys. Rev. B **57**, R9447 (1998).
[19]M. Colocci, M. Gurioli, and J. Martinez Pastor, J. Physique IV **3**, 3 (1993).
[20]L. C. Andreani, F. Tassone, and F. Bassani, Solid State Commun. **77**, 641 (1991).
[21]D. S. Citrin, Phys. Rev. B **47**, 3832 (1993).
[22]E. L. Ivchenko and A. V. Kavokin, Fiz. Tverd. Tela **34**, 1815 (1992); Sov. Phys. Solid State **34**, 968 (1992).
[23]J. J. Hopfield, J. Phys. Chem. Solids **15**, 97 (1960).
[24]J. Massies, C. Deparis, C. Neri, G. Neu, Y. Chen, B. Gil, P. Auvray, and A. Regreny, Appl. Phys. Lett. **55**, 2605 (1989).
[25]Y. P. Varshni, Physica **34**, 149 (1967).
[26]There is an unfortunate typo in page 642, second column, second line of Ref. 20. The correct equation is $\tau_0 = \frac{1}{2\Gamma_0}$. This was corrected in "Optical transitions, excitons, and Polaritons in bulk, and low dimensional semiconductor structures," by L. C. Andreani in *Confined Electrons and Photons*, NATO ASI Series, Series B: Physics, vol. **340**, pages 57-112, edited by Elias Burstein and Claude Weisbuch (Plenum Press, New York, 1995). There is a similar obvious typo in Ref. 18, page R9449, second column, line 18 from the bottom.
[27]Q. M. Yan, P. Rinke,M. Winkelnkemper, A. Qteish, D. Bimberg, M. Scheffler, and C. G. Van de Walle, Semiconductors Science and Technology **26**, 014037 (2011).
[28]*Data in science and technology, semiconductors other than group IV elements and III-V compounds*, edited by O. Madelung (Springer Verlag, Berlin, Heidelberg, 1992), p. 26.
[29]M. Zamfirescu, A. Kavokin, B. Gil, G. Malpuech, and M. Kaliteevskii, Phys. Rev. B **65**, 161205(R) (2002).
[30]C. Klingshirn, J. Fallert, H. Zhou, J. Sartor, C. Thiele, F. Maier-Flaig, D. Schneider, and H. Kalt, Phys. Status Solidi B **247**, 1424 (2010).
[31]S. Faure, T. Guillet, P. Lefebvre, T. Bretagnon, and B. Gil, Phys. Rev. B **78**, 235323 (2008).
[32]T. V. Shubina, M. M. Glazov, N. A. Gippius, A. A. Toropov, D. Lagarde, P. Disseix, J. Leymarie, B. Gil, G. Pozina, J. P. Bergman, and B. Monemar, Phys. Rev. B **84**, 075202 (2011).